ACCSCIENCE PUBLISHING

International Journal of Bioprinting

RESEARCH ARTICLE

Low-concentration GOQD-functionalized Ti6Al4V scaffolds enhance osteogenesis and angiogenesis for vascularized bone regeneration

Duoling Xu[1,2†], Song Yang[3†], Chao Wang[4†], Shujun Li[5], Wentao Hou[5], Jie Wu[1,2], Leyi Liu[1,2], Dongsheng Yu[1,2], Huancai Lin[1,2*], and Wei Zhao[1,2*]

[1]Hospital of Stomatology, Guanghua School of Stomatology, Sun Yat-sen University, Guangzhou, Guangdong, China

[2]Guangdong Provincial Key Laboratory of Stomatology, Sun Yat-sen University, Guangzhou, Guangdong, China

[3]Fujian Key Laboratory of Oral Diseases, Fujian Provincial Engineering Research Center of Oral Biomaterial and Stomatological Key Laboratory of Fujian College and University, Department of Prosthodontics, School and Hospital of Stomatology, Fujian Medical University, Fuzhou, Fujian, China

[4]Departments of Oral Biology, College of Dentistry, University of Illinois Chicago, Chicago, IL, United States of America

[5]Institute of Metal Research, Chinese Academy of Sciences, Shenyang, Liaoning, China

[†]These authors contributed equally to this work.

***Corresponding authors:**
Huancai Lin
(linhc@mail.sysu.edu.cn)

Wei Zhao
(zhaowei3@mail.sysu.edu.cn)

Citation: Xu D, Yang S, Wang C, *et al*. Low-concentration GOQD-functionalized Ti6Al4V scaffolds enhance osteogenesis and angiogenesis for vascularized bone regeneration. *Int J Bioprint*. 2025;11(5):266-283. doi: 10.36922/IJB025290286

Received: June 15, 2025
1st revised: July 14, 2025
2nd revised: July 31, 2025
Accepted: July 31, 2025
Published online: July 31, 2025

Abstract

Graphene oxide quantum dots (GOQDs) possess excellent biocompatibility and have demonstrated potential to enhance osteogenesis and angiogenesis. The objective of this work was to construct Ti6Al4V porous scaffolds modified with different GOQD concentrations and investigate their influence on osteogenesis and angiogenesis. Porous Ti6Al4V scaffolds were coated with GOQDs at concentrations of 0.1, 1, and 10 μg/mL. The proliferation and adhesion of bone marrow mesenchymal stem cells (BMSCs) and human umbilical vein endothelial cells (HUVECs) on these scaffolds were evaluated using CCK-8 assay, immunofluorescence staining, and real time-polymerase chain reaction (RT-PCR). *In vivo* bone regeneration and angiogenesis were assessed through micro-computed tomography imaging and tissue section staining analysis. The results demonstrated successful deposition of GOQDs and the presence of characteristic functional groups. *In vitro* assays demonstrated that scaffolds coated with 0.1 μg/mL GOQDs significantly promoted the osteogenic/angiogenic differentiation of BMSCs and HUVECs. *In vivo* experiments revealed that the 0.1 μg/mL GOQDs-coated scaffold (GQ@TC4) significantly enhanced bone formation and vascularization after 12 weeks. These findings suggest that Ti6Al4V biomimetic porous scaffolds functionalized with an optimal concentration (0.1 μg/mL) of GOQDs can effectively promote both osteogenesis and angiogenesis, offering a promising strategy for bone defect repair.

Keywords: Bone marrow mesenchymal stem cells; Graphene oxide quantum dots; Human umbilical vein endothelial cells; Ti6Al4V biomimetic porous scaffolds; Vascularized bone regeneration

1. Introduction

Bone defects resulting from tumors, infections, trauma, and congenital deformities are common in oral and maxillofacial surgery. Achieving efficient and predictable bone regeneration remains a major clinical challenge.[1] Currently, vascularized autografts or allografts are widely used for bone defect repair. However, their application is limited by donor site availability, associated complications, and delayed bone healing. Moreover, systemic conditions, such as diabetes and local inflammation, can significantly impair the regenerative capacity of bone tissue.[2,3]

An ideal bone graft substitute should meet the following criteria: mechanical properties compatible with native bone (*e.g.*, high strength and appropriate elastic modulus) to provide structural support and biomechanical stimulation; excellent osteogenic and angiogenic capabilities to facilitate vascularized bone regeneration; and superior interfacial compatibility to promote implant–host bone integration. To date, no single material fully meets the requirements for repairing large-scale bone defects.

Ti6Al4V alloy scaffolds have been widely utilized in orthopedics and maxillofacial surgery.[4–7] However, their bioinert surfaces tend to form fibrous interfaces with surrounding bone tissue, compromising osseointegration.[8] Furthermore, the elastic modulus of Ti6Al4V greatly exceeds that of native bone, which may lead to stress shielding effects, implant instability, and eventual failure.[9,10]

Studies have demonstrated that introducing porous architecture into Ti6Al4V scaffolds can effectively reduce their bulk elastic modulus and significantly enhance the adhesion, proliferation, and differentiation of osteoblasts by optimizing pore parameters, such as pore size, porosity, and irregularity.[11,12] Among these, trabecular bone-mimicking irregular porous structures exhibit superior biological performance due to their closer resemblance to the microarchitecture of native bone.[13,14] For instance, Kapat *et al.*[14] reported that an irregular foam scaffold with 70% porosity significantly enhanced osteogenic potential. Our prior study also demonstrated that irregular porous scaffolds with an average pore size of 525 μm effectively enhanced both osteogenesis and angiogenesis.[15–17] Similarly, Jung *et al.*[18,19] have systematically optimized pore geometry and structural characteristics of porous titanium scaffolds to enhance osteoconductivity and mechanical properties, offering valuable insights for scaffold design. However, despite the improved mechanical performance and cellular response afforded by porosity, the intrinsic bioinertness of Ti6Al4V still limits its ability to induce vascularized bone regeneration, necessitating further surface functionalization.

Surface modification of titanium scaffolds includes both physical and chemical approaches, such as coating, electrochemical treatment, and chemical vapor deposition.[20,21] Among these, functional coating by spraying is an efficient physical strategy using materials like metal nanoparticles, hydroxyapatite, or graphene derivatives.[22–24] Graphene coatings have been verified to enhance the bioactivity of titanium-based scaffolds, improve the osteogenic differentiation of bone marrow mesenchymal stem cells (BMSCs), and reduce immune rejection and inflammation.[25] Graphite oxide quantum dots (GOQDs), a graphene derivative, exhibit quantum size effects and good water dispersibility, along with lower cytotoxicity and superior biocompatibility compared to conventional GO.[26,27] Our previous work confirmed that GOQDs significantly promote the proliferation and osteogenic differentiation of both deciduous dental pulp stem cells and mesenchymal stem cells.[28,29] Furthermore, the biological activity of GOQDs is dose-dependent. While low concentrations are beneficial for maintaining cell viability and enhancing osteogenic differentiation, concentrations exceeding 10 μg/mL have been reported to inhibit cell proliferation.[30,31] Given our earlier results indicating that 0.1 and 1 μg/mL GOQDs enhance BMSC behavior,[32] these concentrations were selected as low-dose groups, with 10 μg/mL serving as the high-dose reference in this study.

Based on this foundation, we hypothesize that constructing an optimal concentration of GOQDs coating on biomimetic trabecular porous Ti6Al4V scaffolds can synergistically enhance mechanical compatibility and biofunctionality, providing both structural support and osteogenic/angiogenic stimulation. Therefore, this study aims to functionalize biomimetic porous Ti6Al4V scaffolds with low-concentration GOQDs, assess their effects through co-culture with BMSCs and human umbilical vein endothelial cells (HUVECs), and validate the osteogenic and angiogenic efficacy via *in vivo* experiments. The results are expected to provide new insights and theoretical guidance for the design of advanced bone graft substitutes and promote their clinical translation.

2. Materials and methods

2.1. Preparation of GOQD-modified biomimetic scaffolds

The GOQD stock solution (1 mg/mL) (Nanjing XFNANO Materials, China) was ultrasonicated to achieve homogeneous dispersion and then diluted with deionized water. The final concentrations of GOQDs (0.1, 1, and 10 μg/mL) were prepared for subsequent experiments. Ti6Al4V biomimetic porous scaffolds with an actual pore size of 525 μm were printed using an electron beam melting

(EBM) system (A1, ARCAM, Sweden), as previously reported.[16] For *in vitro* studies, the scaffolds were 10 mm in diameter and 2 mm in thickness; for *in vivo* studies, the scaffolds measured 5 mm in diameter and 8 mm in thickness (Figure 1A). The spray-coating method was used to prepare GOQD coatings with different concentrations on the surface of Ti6Al4V biomimetic porous scaffolds. Four experimental groups were established: (i) control: untreated Ti6Al4V porous scaffolds; (ii) GQ0.1@TC4: Ti6Al4V scaffolds coated with 0.1 μg/mL GOQD solution; (iii) GQ1@TC4: Ti6Al4V scaffolds coated with 1 μg/mL GOQD solution; and (iv) GQ10@TC4: Ti6Al4V scaffolds coated with 10 μg/mL GOQD solution.

Ti6Al4V porous scaffolds with an actual pore size of 525 μm were selected and cleaned three times with anhydrous ethanol to remove surface dust and grease. The scaffolds were then dried and subjected to plasma treatment to enhance surface hydrophilicity and coating adhesion. After treatment, the scaffolds were placed on a 100°C heating platform, and the pre-prepared GOQD solutions (0.1, 1, and 10 μg/mL) were uniformly sprayed onto the scaffold surfaces using a spray gun. As the solvent evaporated, a uniform GOQD coating was formed. Finally, the coated scaffolds were baked in a 100°C oven for 2–3 h to obtain GOQD-modified Ti6Al4V porous scaffolds (Figure 1A).

2.2. GOQD-modified biomimetic scaffold characterization

X-ray powder diffraction (XRD) was carried out using a Supernova diffractometer (Japan) to determine the phase composition of the samples. The scanning was performed over a 2θ range of 5°–80°, employing Cu Kα radiation (λ = 1.5411 Å) as the source. X-ray photoelectron spectroscopy (XPS) (Nexsa, Thermo Fisher Scientific, USA) was utilized to assess the surface elemental composition of the samples. Fourier transform infrared spectroscopy (FTIR) (Nicolet NXR 9650, Thermo Fisher Scientific, USA) was used to detect the functional groups present in the GOQDs, with spectra recorded in the range of 500–4000 cm^{-1}.

2.3. Effect of modified biomimetic scaffold extracts on the proliferation of BMSCs and HUVECs

2.3.1. Preparation of GOQD-modified biomimetic scaffold conditioned medium

BMSCs were extracted from Sprague–Dawley rats. Upon reaching approximately 80% confluency, the cells were collected by treatment with 0.25% trypsin-EDTA (Gibco, USA). The BMSCs (passage 3) were used for further experiments. HUVECs were purchased from ScienCell™ Research Laboratories (USA). The culture conditions for HUVECs were maintained similarly to those applied for BMSCs.

For the preparation of conditioned medium, BMSCs or HUVECs were seeded onto the scaffolds and incubated in their respective complete media for 72 h. After incubation, the supernatant was collected and then stored at 4°C until it was used for subsequent experiments.

2.3.2. Effect of GOQD-modified biomimetic scaffold extracts on the proliferation of BMSCs

At predetermined time points, cell proliferation and viability were assessed accordingly. The cell proliferation rate in each group was evaluated using Cell Counting Kit-8 (CCK8) (Dojindo, Japan). Cells were incubated with medium containing 10% (v/v) CCK-8 reagent (Dojindo Laboratories, Japan) for 60 min in the dark. Subsequently, the absorbance at 450 nm was detected using a microplate reader (Bio-Tek, UK) to assess cell proliferation.

The cells were treated with a working solution containing calcein AM and ethidium homodimer-1 (Invitrogen, USA). After incubation for 30 min at 37°C, fluorescence signals were tested using a confocal laser scanning microscope (LSM780, Zeiss, Germany).

The samples were incubated with phalloidin (Solarbio, China) for 30 min at 37°C to stain the F-actin cytoskeleton. The nuclear staining was carried out using 4′,6-diamidino-2-phenylindole (Solarbio, China).

2.3.3. Effect of GOQD-modified biomimetic scaffold extracts on the proliferation of HUVECs

HUVECs at passage 3 were cultured in complete Dulbecco's Modified Eagle's Medium (DMEM) for 2 days prior to treatment. The medium was subsequently replaced with conditioned medium derived from the GOQD-modified scaffold groups. CCK-8 assay and immunofluorescence staining were performed as described in **Section 2.3.2**.

2.3.4. Effect of GOQD-modified biomimetic scaffold extracts on the angiogenic potential of HUVECs

HUVECs were digested with trypsin, centrifuged, and resuspended in complete DMEM. HUVECs were divided into four experimental groups: control, GQ0.1@TC4, GQ1@TC4, and GQ10@TC4. When cell monolayers reached approximately 80% confluence, a linear wound was created using a 1000 μL pipette tip held perpendicular to the plate surface. The migration area was then quantified using ImageJ software to assess wound closure efficiency.

Cell migration was evaluated using a Transwell system (8 μm pore size, Corning, USA). A total of 3×10^4 HUVECs suspended in serum-free medium were added to the upper chamber, while 750 μL of complete F-12K medium (without antibiotics) was placed in the lower chamber as

a chemoattractant. The migrated cells were then imaged using an inverted microscope and quantitatively analyzed with ImageJ software.

The capacity of HUVECs to form capillary-like structures was assessed using a Matrigel-based tube formation assay. A 96-well plate was precooled on ice, and 50 μL of Matrigel (Corning, USA) was added to each well. HUVECs, pretreated with the scaffold extracts for 24 h, were then collected, counted, and seeded onto the solidified Matrigel. After 24 h of incubation, tube formation was observed. The total tube length and branch points were analyzed using ImageJ software.

2.4. Effects of GOQD-modified biomimetic scaffolds on cell adhesion and osteogenic/angiogenic differentiation of BMSCs and HUVECs

2.4.1. Effects of GOQD-modified biomimetic scaffolds on the adhesion and osteogenic differentiation of BMSCs

The morphological characteristics and adhesion of BMSCs on GOQD-modified biomimetic scaffolds were observed using scanning electron microscopy (SEM) (Nexsa, Thermo Fisher Scientific, USA). To evaluate the osteogenic differentiation potential of BMSCs, the expression levels of osteogenesis-related genes (*Runx2*, *Bmp2*, *Ocn*, and *Alp*) were analyzed by real time-polymerase chain reaction (RT-PCR) after culture on GOQD-modified biomimetic scaffolds. The primer sequences used are listed in **Table S1**.

2.4.2. Effects of GOQD-modified biomimetic scaffolds on the adhesion and angiogenic differentiation of HUVECs

The morphology and adhesion behavior of HUVECs on GOQD-modified biomimetic scaffolds were assessed using SEM. To assess the angiogenic potential of HUVECs, the vascular endothelial growth factor (VEGF) and hypoxia-inducible factor 1-alpha (HIF-1α) were detected by RT-PCR, following culture on GOQD-modified scaffolds. The primer sequences are listed in **Table S2**.

2.5. *In vivo* evaluation of osteogenic and angiogenic performance of GOQD-modified biomimetic scaffolds

In vivo experiments were conducted using 12 adult male New Zealand white rabbits (weighing 2.5–3.0 kg each). The animal procedures strictly adhered to relevant ethical guidelines and were approved by the Institutional Animal Care and Use Committee of Sun Yat-sen University (Approval No. SYSU-IACUC-2019-000169).

Two types of porous biomimetic scaffolds (diameter: 5 mm; height: 8 mm) were implanted into the femoral condyles of rabbits. Group 1 (control) consisted of Ti6Al4V scaffolds with a solid core and an irregular porous outer surface with a pore size of approximately 525 μm. Group 2 (GQ@TC4) was composed of the same Ti6Al4V scaffold, with the surface coated with GOQDs at the optimal concentration previously identified in **Sections 2.2 and 2.3** for promoting osteogenesis and angiogenesis.

After 3 months of implantation, bone regeneration and neovascularization around the scaffolds were assessed using micro-computed tomography (micro-CT), histological analysis, and immunohistochemical staining.

2.6. Statistical analysis

All data are presented as mean ± standard deviation. To ensure the reliability of the statistical results, sample sizes were determined based on previous studies and pilot experiments to achieve a statistical power greater than 80% at a significance level of 0.05. The normality of the data was assessed using the Shapiro–Wilk test. For comparisons among multiple groups, one-way analysis of variance was performed, followed by Tukey's Honestly Significant Difference test as a post hoc analysis to identify specific group differences. A p-value <0.05 was considered statistically significant. All experiments were conducted in triplicate or more.

3. Results

3.1. GOQD-modified biomimetic scaffold surface characterization

To evaluate the effects of GOQDs at different concentrations, biomimetic porous Ti6Al4V scaffolds were coated with GOQDs at 0, 0.1, 1, and 10 μg/mL. These four groups were designated as control, GQ0.1@TC4, GQ1@TC4, and GQ10@TC4, respectively. After conducting the *in vitro* experiments, the optimal GOQDs concentration was selected for subsequent *in vivo* evaluation. For the animal study, Ti6Al4V scaffolds without GOQD coating and those coated with the optimal concentration of GOQDs were designated as control and GOQDs@TC4, respectively. The fabricated scaffold samples are displayed in Figure 1A.

Figure 1B presents the XRD patterns of the GQ0.1@TC4, GQ1@TC4, and GQ10@TC4 scaffolds. All samples exhibited distinct diffraction peaks at 2θ values of 35.2°, 38.3°, 40.5°, 54.3°, 63.1°, and 72.2°, which correspond to characteristic peaks of Ti6Al4V. Additionally, a prominent diffraction peak was observed at 2θ = 10.2° in the GQ10@TC4 group, indicating the successful incorporation of GOQDs on the scaffold surface. No extraneous peaks were detected in the XRD spectra, suggesting the absence of impurities introduced during fabrication.

The XPS analysis (Figure 1C and D) confirmed the presence of characteristic peaks for C1s, O1s, and

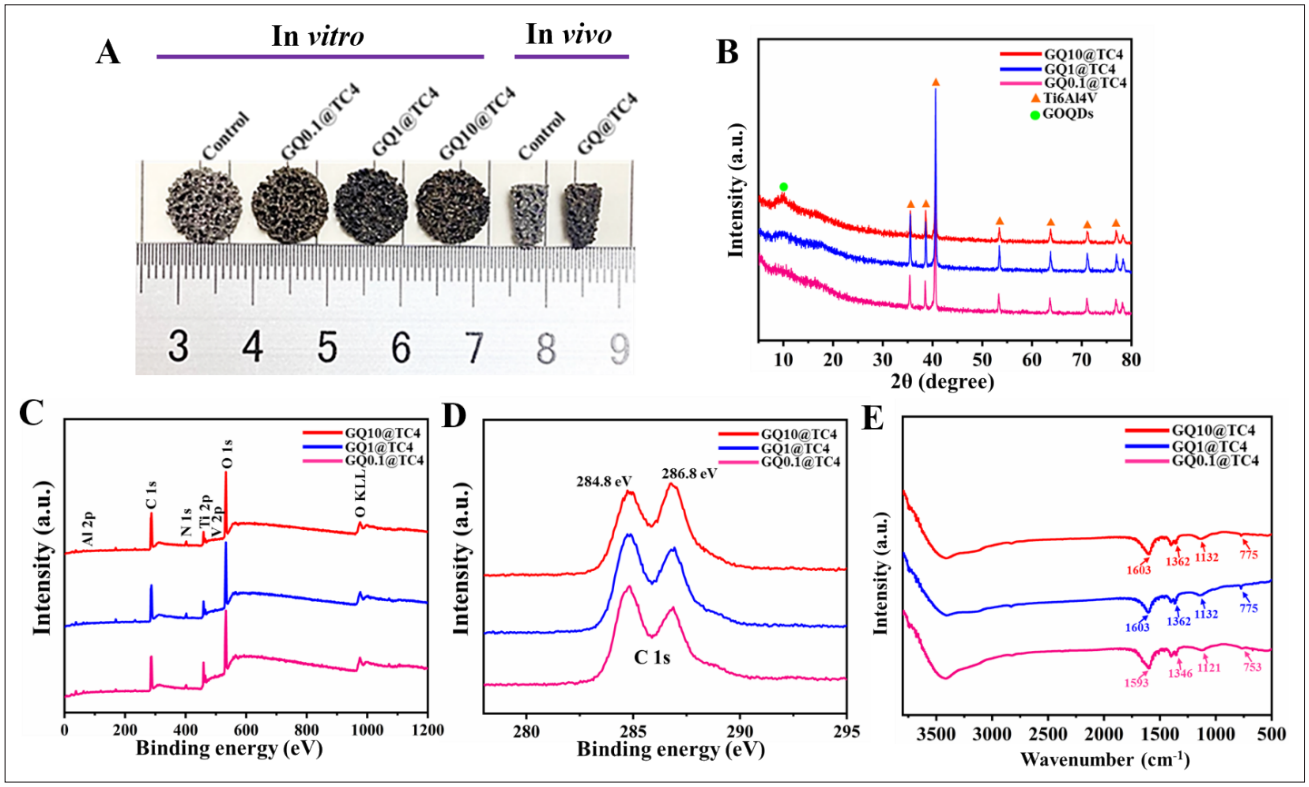

Figure 1. Surface characteristics of the biomimetic porous Ti6Al4V scaffolds. (A) Biomimetic porous scaffolds fabricated by EBM for *in vitro* and *in vivo* experiments. (B) XRD patterns of the biomimetic porous Ti6Al4V scaffolds. (C) XPS survey spectra of scaffolds modified with different concentrations of GOQDs. (D) High-resolution XPS spectra of the C1s region on the scaffold surfaces. (E) FTIR spectra of the biomimetic porous Ti6Al4V scaffolds. Abbreviations: EBM, electron beam melted; FTIR, Fourier transform infrared spectroscopy; XPS, X-ray photoelectron spectroscopy; XRD, X-ray powder diffraction.

Ti2p elements, further validating the successful surface modification with GOQDs. The incorporation of GOQDs altered the surface chemical composition of Ti6Al4V, which may contribute to enhanced biocompatibility.

FTIR results (Figure 1E) demonstrated typical absorption bands in the range of 1100–1600 cm^{-1} that correspond to C=O stretching vibrations, as well as a broad O–H stretching peak around 3450 cm^{-1}. These findings confirm the successful attachment of GOQDs onto the Ti6Al4V scaffold surface. The increased presence of hydroxyl, carbonyl, and conjugated double bond groups introduced by GOQDs may enhance the surface bioactivity and improve cellular interactions.

3.2. Effects of GOQD-modified biomimetic scaffold extracts on the proliferation of BMSCs and HUVECs

3.2.1. Effects on BMSC proliferation

According to the Raman spectra of the GQ0.1@TC4 scaffolds before and after immersion in culture medium for 2 weeks in the preliminary experiment of this study (Figure S1), GOQDs were still coating on the TC4 surface, indicating good stability of the GOQDs coating on the biomimetic scaffold and supporting its suitability for subsequent cell experiments. The proliferation results of BMSCs cultured with scaffold extracts are displayed in Figure 2C. Within the concentration range of 0.1–10 μg/mL, BMSC proliferation decreased with increasing GOQD concentration. Notably, the GQ0.1@TC4 group exhibited significantly higher proliferation at days 1, 3, 5, and 7 compared to the other groups ($p < 0.001$).

Live/dead staining results are presented in Figure 2A. As the GOQD concentration increased, the number of viable BMSCs decreased. Both GQ0.1@TC4 and GQ1@TC4 groups displayed a relatively high number of live cells, with GQ0.1@TC4 demonstrating the highest cell viability and strongest fluorescence intensity.

Immunofluorescence staining results are presented in Figure 2B. A gradual decline in BMSC number was observed with increasing GOQD concentrations. The GQ0.1@TC4 group had the highest cell count with regular, spindle-shaped morphology. In contrast, the GQ10@

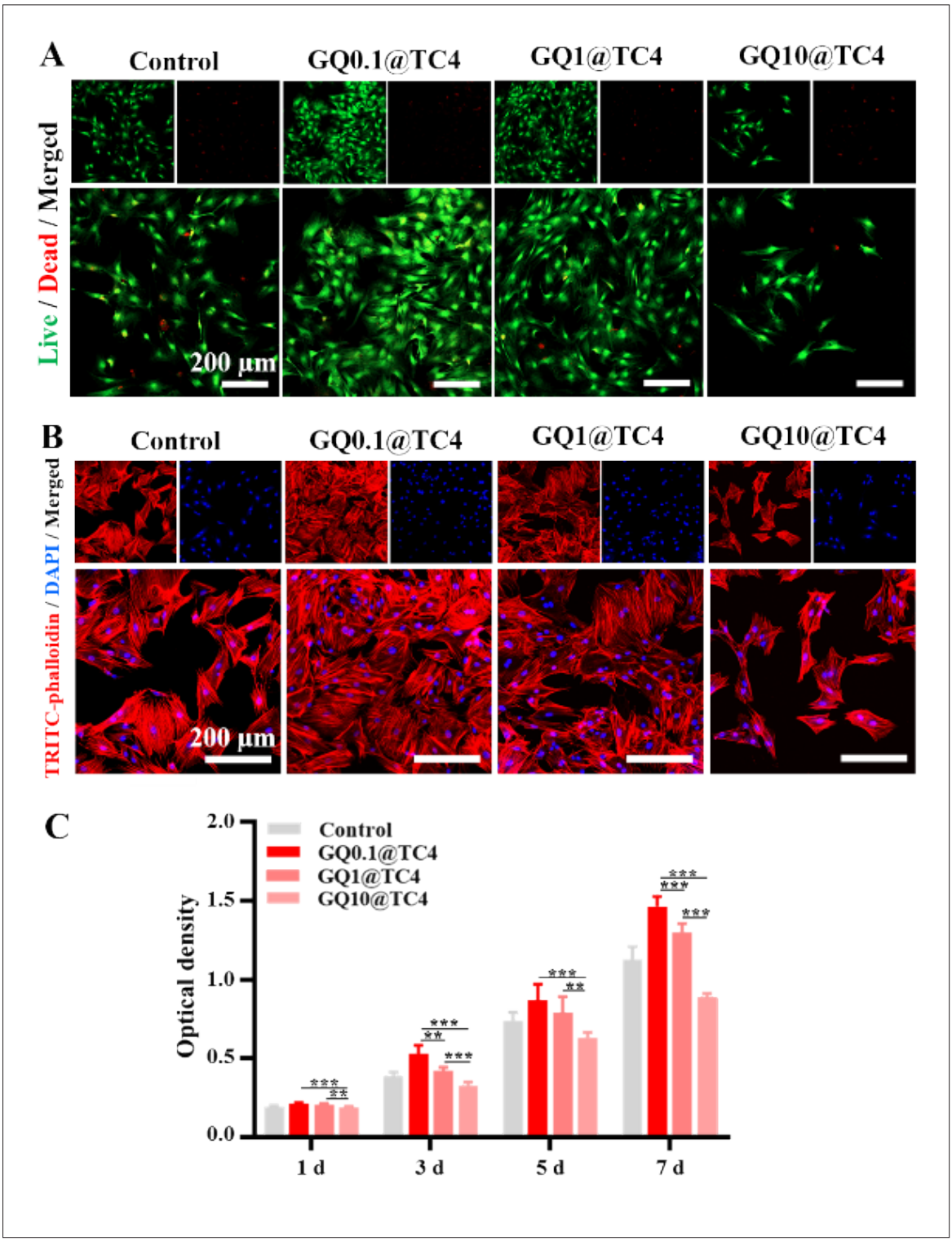

Figure 2. Effects of GOQD-modified biomimetic scaffold extracts on BMSC proliferation. (A) Confocal laser scanning microscopy images of live/dead staining of BMSCs co-cultured with extracts from four groups of titanium alloy scaffolds. (B) Confocal images of immunofluorescence staining, featuring the cytoskeletal morphology of BMSCs after 3 days of co-culture; the red stain indicates F-actin filaments, while the blue stain indicates nuclei. (C) Proliferation of BMSCs co-cultured with extracts from the four scaffold groups for 1, 3, 5, and 7 days, assessed by the CCK-8 assay. ($n = 3$; $^{**}p < 0.01$ and $^{***}p < 0.001$, compared to the control). Scale bars: 200 μm (A and B). Abbreviations: BMSC, bone marrow mesenchymal stem cells; GOQD, graphite oxide quantum dots.

TC4 group displayed the fewest cells, with shrunken and irregular cytoskeletal structures.

3.2.2. Effects on HUVEC proliferation

The proliferation results of HUVECs cultured with scaffold extracts are presented in Figure 3C. Similar to BMSCs, HUVEC proliferation declined with increasing GOQD concentration. The GQ0.1@TC4 group demonstrated significantly higher proliferation at days 1, 3, 5, and 7 compared to other groups ($p < 0.001$).

Immunofluorescence staining (Figure 3A) revealed a decrease in HUVEC number with increasing GOQD concentration. The GQ0.1@TC4 group had the highest number of HUVECs, predominantly exhibiting an oval morphology and well-organized cytoskeletal structures.

As displayed in Figure 3B and D, after 24 h of treatment with scaffold extracts, the GQ0.1@TC4 group exhibited significantly enhanced migration of HUVECs compared to the GQ1@TC4 and GQ10@TC4 groups ($p < 0.05$). The wound area in the GQ0.1@TC4 group was nearly completely closed within 24 h. After 24 h of treatment, the number of HUVECs migrating through the Transwell membrane was higher in the GQ0.1@TC4 group (635 ± 59) compared to the GQ1@TC4 (428 ± 47) and GQ10@TC4 (149 ± 56) groups ($p < 0.05$) (Figure 4A and C). As presented in Figure 4B and D, after 24 h of extract treatment, HUVECs in the GQ0.1@TC4 group formed significantly longer tube-like structures than those in the GQ1@TC4 and GQ10@TC4 groups ($p < 0.05$). The total tube length in the GQ0.1@TC4 group (2867 ± 49 μm) was approximately three times that of the GQ10@TC4 group (1054 ± 55 μm). Consistently, in our preliminary experiment, co-culturing different GQ@TC4 groups with human bone marrow mesenchymal stem cells (HMSCs) yielded nearly identical results (Figure S2), further confirming the superior pro-migratoryand pro-angiogenic effects of the GQ0.1@TC4 group.

3.3. Effects of GOQD-modified biomimetic scaffolds on BMSC/HUVEC adhesion and osteogenic/angiogenic differentiation

3.3.1. Effects of GOQD-modified scaffolds on BMSC adhesion and osteogenic differentiation

The SEM images featured in Figure 5A indicate that BMSCs adhered to the scaffold surface and exhibited elongated spindle-like morphology. After 7 days of co-culture with biomimetic porous scaffolds modified with varying concentrations of GOQDs, the number of adherent BMSCs decreased with increasing GOQD concentration. Among all groups, the GQ0.1@TC4 group demonstrated the highest degree of cell adhesion on the scaffold surface.

The RT-PCR analysis (Figure 5C) revealed that after 7 days of co-culture, the expression levels of osteogenic-related genes (*Bmp2*, *Ocn*, and *Alp*) were significantly higher in the GQ0.1@TC4 group compared to the GQ1@TC4 and GQ10@TC4 groups ($p < 0.05$), indicating enhanced osteogenic differentiation.

3.3.2. Effects of GOQD-modified scaffolds on HUVEC adhesion and angiogenic differentiation

The SEM images presented in Figure 5B indicate that HUVECs adhered to the scaffold surface in both scattered and clustered formations. After 7 days of co-culture, the GQ0.1@TC4 group exhibited the greatest number of adherent cells, with cells forming confluent layers and overlapping in some regions, compared to the other groups.

The RT-PCR results (Figure 5D) demonstrated that the mRNA expression levels of angiogenesis-related genes (*VEGF* and *HIF1A*) were significantly higher in the GQ0.1@TC4 group than in the GQ1@TC4 and GQ10@TC4 groups ($p < 0.05$), suggesting that low-concentration GOQD modification promotes angiogenic differentiation of HUVECs.

3.4. *In vivo* osteogenic and angiogenic evaluation of GOQD-functionalized biomimetic scaffolds

Based on *in vitro* osteogenesis and angiogenesis experiments conducted using both extract and co-culture methods, the GQ0.1@TC4 group exhibited the most favorable outcomes in promoting BMSC adhesion, proliferation, and differentiation, as well as the strongest pro-angiogenic effects on HUVECs. Therefore, the GQ0.1@TC4 scaffold was selected for subsequent *in vivo* studies. To evaluate its osteogenic and angiogenic capacity *in vivo*, a comparative analysis was performed between the GQ0.1@TC4 scaffold and a biomimetic scaffold without GOQD modification using micro-CT, histological staining, and immunohistochemistry. In this section, the scaffold without GOQDs is referred to as the control, while the Ti6Al4V scaffold coated with 0.1 μg/mL GOQDs is denoted as GQ@TC4.

3.4.1. Micro-CT analysis

The micro-CT results (Figure 6A) revealed that at 4 weeks post-implantation in rabbit femurs, more bone tissue had formed around the GQ@TC4 scaffolds, and the gaps between the scaffold and cortical bone were significantly reduced. The bone volume fraction (BV/TV) of the GQ@TC4 group reached 4.85 ± 1.08% (Figure 6B). By week 12, the bone coverage on the scaffold surface had notably increased compared to week 4. The GQ@TC4 scaffolds demonstrated close integration with surrounding cortical bone, with a higher proportion of newly formed yellow-colored bone tissue. The BV/TV in the GQ@TC4 group

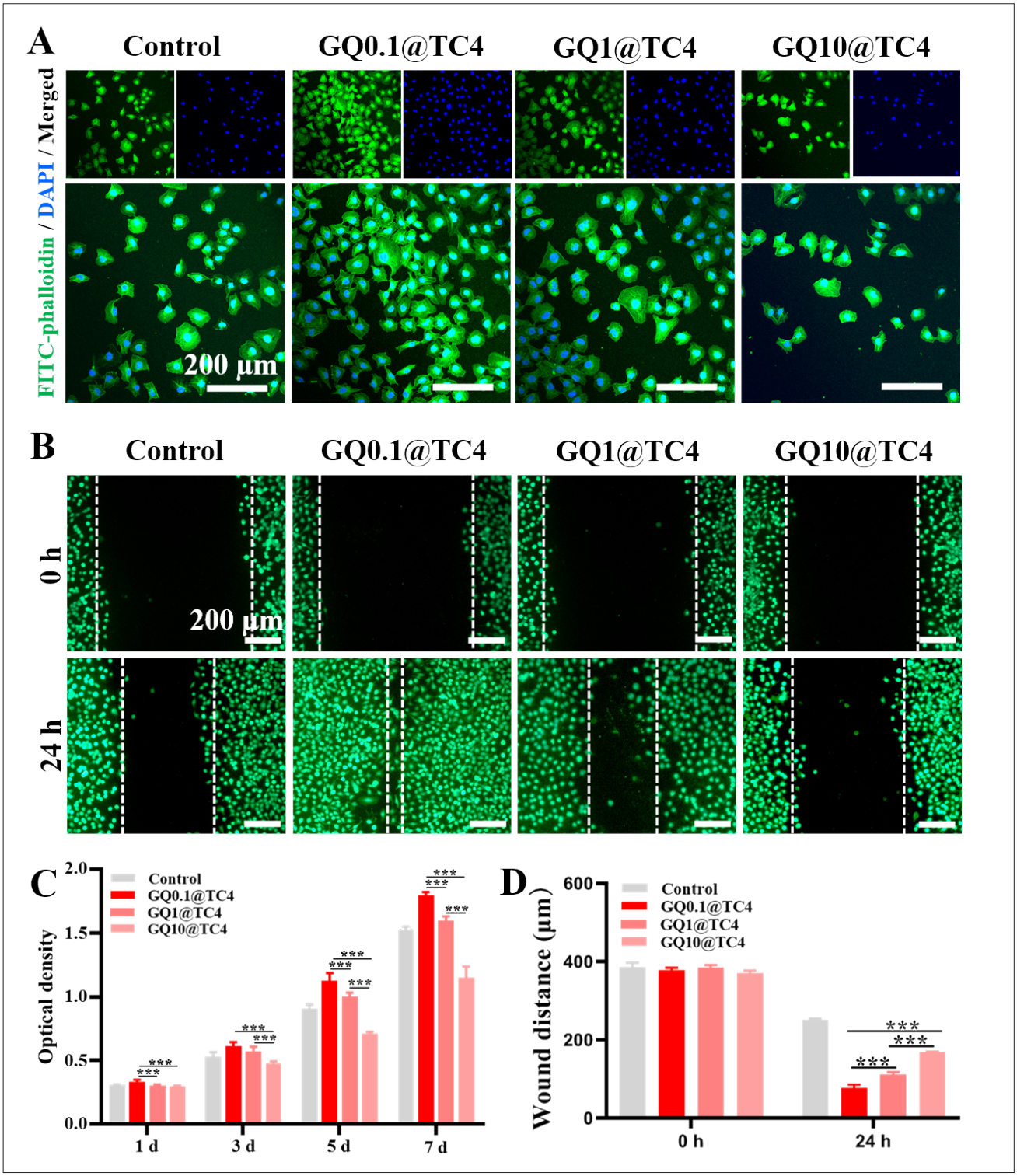

Figure 3. Effects of GOQD-modified biomimetic scaffold extracts on HUVEC proliferation and angiogenic capacity. (A) Confocal laser scanning microscopy images of immunofluorescence staining, displaying HUVEC morphology after co-culture with extracts from four groups of titanium alloy scaffolds for 3 days; the green stain indicates F-actin filaments, while the blue stain indicates nuclei. (B) Fluorescence images of scratch assays, indicating HUVEC migration at 0 and 24 h after treatment with the four scaffold extracts. (C) Proliferation of HUVECs co-cultured with the scaffold extracts for 1, 3, 5, and 7 days, assessed using the CCK-8 assay. (D) Quantitative bar graph of HUVEC migration distances. $n = 3$; ***$p < 0.001$ compared to the control. Scale bars: 200 μm (A and C). Abbreviations: GOQD, graphite oxide quantum dots; HUVEC, human umbilical vein endothelial cells.

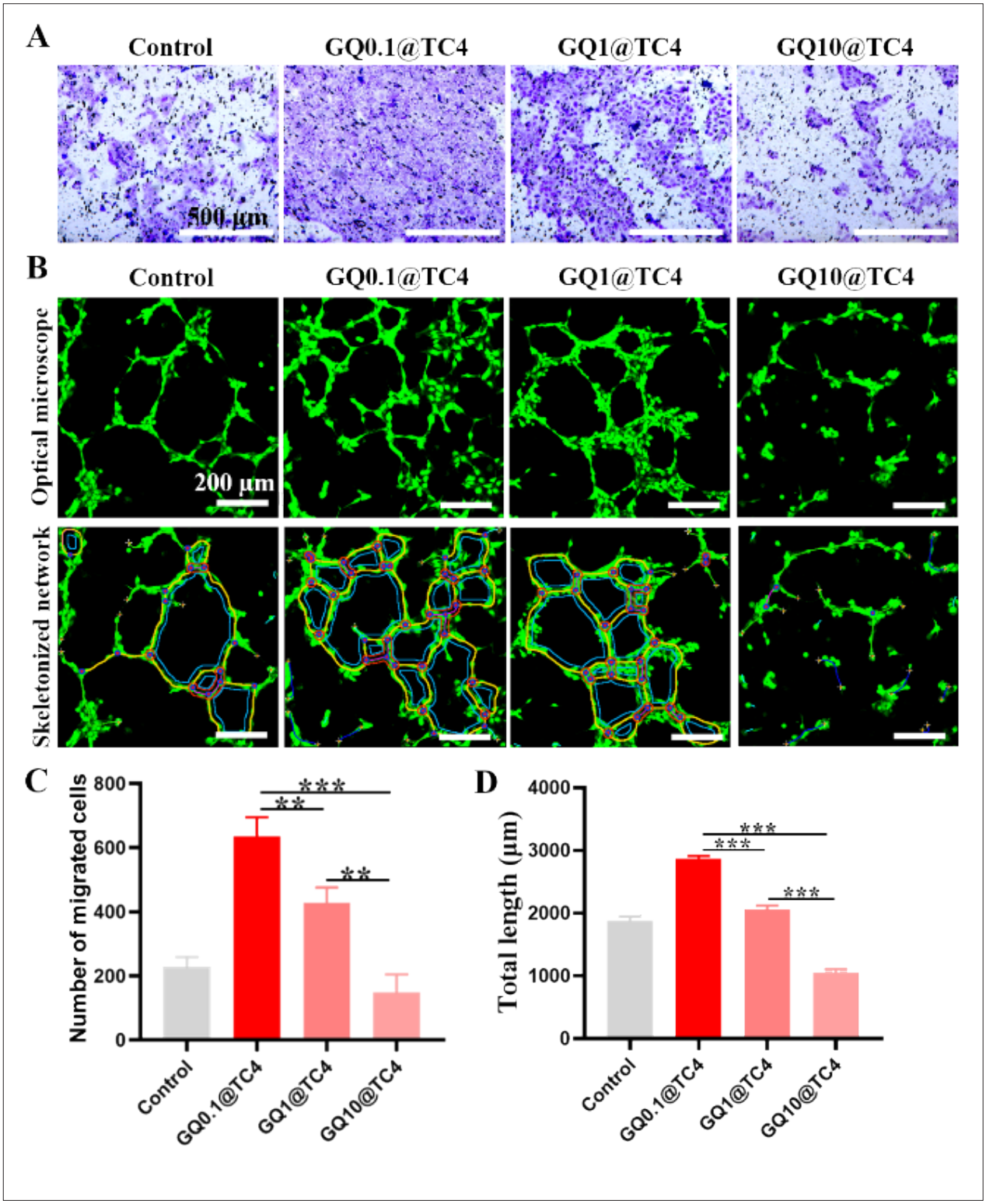

Figure 4. Transwell migration and tube formation assays of HUVECs after 24 h treatment with scaffold extract from the four groups. (A) Representative images of migrated HUVECs stained after the Transwell assay. (B) Fluorescence microscopy images displaying tube formation by HUVECs after treatment with different scaffold extracts. (C) Quantitative analysis of the number of HUVECs that migrated through the membrane. (D) Quantification of total tube length formed by HUVECs. $n = 3$; $^{**}p < 0.01$ and $^{***}p < 0.001$, compared to the control. Scale bars: 500 μm (A); 200 μm (C). Abbreviation: HUVEC, human umbilical vein endothelial cells.

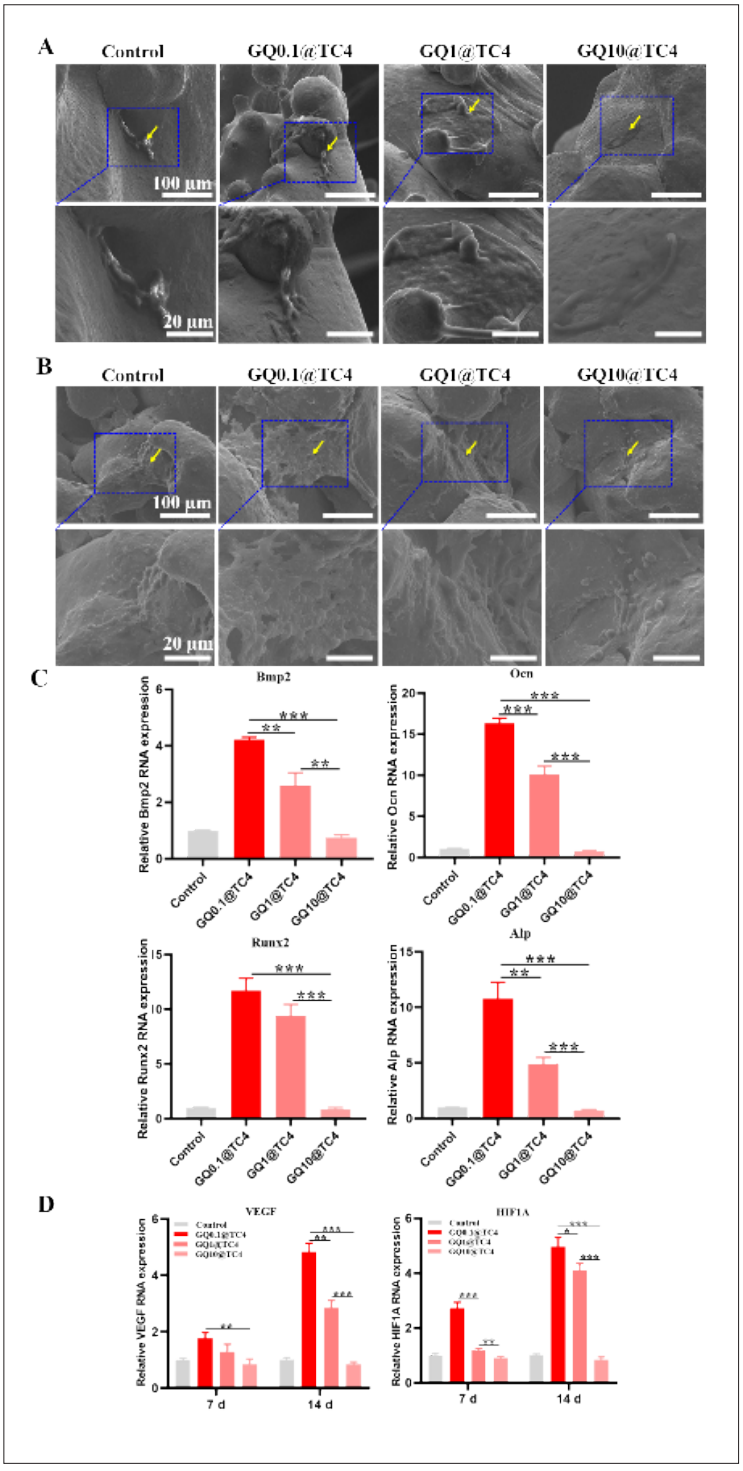

Figure 5. Cell adhesion and morphology on the surface of GOQD-modified biomimetic scaffolds observed by SEM, and RT-PCR analysis of osteogenic and angiogenic gene expression. (A) SEM images displaying cell adhesion on the scaffolds after 7 days of culture. Yellow arrows indicate BMSCs adhering and growing on the scaffold surface. (B) SEM images displaying HUVECs adhered to the scaffold surface after 7 days of culture. Yellow arrows indicate attached HUVECs. (C) RT-PCR analysis of osteogenic gene expression (*Bmp2*, *Ocn*, *Runx2*, and *Alp*) in BMSCs cultured on the four groups of Ti6Al4V scaffolds. (D) RT-PCR analysis of angiogenesis-related gene expression (*VEGF* and *HIF1A*) in HUVECs cultured on the four groups of scaffolds. $n = 3$; $^{**}p < 0.01$ and $^{***}p < 0.001$, compared to the control. Scale bars: 100 μm (A and C, top); 20 μm (A and C, bottom). Abbreviations: BMSCs, bone marrow mesenchymal stem cells; HUVECs, human umbilical vein endothelial cells; RT-PCR, real time-polymerase chain reaction; SEM, scanning electron microscope.

reached 43.29 ± 3.26%, significantly higher than that in the control group ($p < 0.05$).

3.4.2. Histological observation

Hematoxylin and eosin (H&E) staining (Figure 6C) revealed the formation of small areas of red-stained bone tissue around the GQ@TC4 scaffolds at week 4 (yellow arrows in Figure 6C). The BV/TV was 3.60 ± 0.68%. By week 12, new bone formation on the scaffold increased markedly, with the GQ@TC4 group exhibiting a BV/TV of 16.72 ± 1.07%, significantly greater than that of the control group ($p < 0.05$) (Figure 6D).

Modified Masson's trichrome staining (Figure 6E) further confirmed these findings. At week 4, limited new bone tissue was observed at the interface between the GQ@TC4 scaffold and host bone (yellow arrows in Figures 6C and E), with a BV/TV of 6.13 ± 0.85%. At week 12, extensive new bone formation was evident, with the newly formed tissue connecting across the scaffold. The BV/TV reached 10.37 ± 1.13% in the GQ@TC4 group, significantly higher than that in the control group ($p < 0.05$) (Figure 6F).

CD31 immunohistochemical staining was used to assess neovascularization. CD31-positive endothelial cells formed round or oval yellow to brown ring-like structures representing vascular lumens (Figure 6G). At week 4, only a few vessels were observed in the control group, while significantly more blood vessels of various diameters were present in the GQ@TC4 group. At week 12, the GQ@TC4 scaffolds exhibited a larger number and diameter of vascular lumens compared to the control group, with statistically significant differences ($p < 0.05$) (Figure 6H).

4. Discussion

Owing to their favorable properties in promoting osteogenesis and angiogenesis, GOQDs have attracted great attention in the fields of orthopedic implants and dental prosthetics.[33,34] As a derivative of graphene oxide (GO), GOQDs have demonstrated promising osteoinductive potential in both *in vitro* and *in vivo* studies.[35,36] However, differences in oxygen content and particle size during GOQD synthesis result in variations in their physicochemical properties. Previous studies have demonstrated that parameters such as the oxygen content, diameter, and thickness of graphene-based materials significantly influence their osteoinductive capabilities.[37–39]

Based on the findings in our previous study,[16] Ti6Al4V scaffolds with irregular porous structures and an average pore size of 525 μm effectively promoted BMSC osteogenic differentiation. In combination with our previous research,[32] which identified the optimal GOQD concentration (0.1 μg/mL) for enhancing BMSC proliferation and differentiation, this study focused on coating Ti6Al4V scaffolds (pore size: 525 μm) with three concentrations of GOQDs. Furthermore, *in vivo* experiments were conducted to assess the scaffolds' capacities for bone and vascular regeneration under appropriate GOQD loading concentration.

As a surface modification strategy for metallic implants, GOQD coating is considered a safe and effective approach.[40] Variations in GOQDs' characteristics, such as particle size and chemical composition, can alter the physicochemical properties of the implant material, including its structure and morphology.[41] In this study, the XRD results (Figure 1B) revealed the presence of characteristic peaks for both Ti6Al4V and GOQDs without any additional impurity peaks, indicating that the coating process did not introduce contaminants. Specifically, Ti6Al4V exhibited a characteristic peak near $2\theta = 40°$, corresponding to the (110) plane, while GOQDs exhibited a peak at $2\theta \approx 10°$, corresponding to the (001) plane. Notably, the intensity of the Ti6Al4V peak varied with increasing GOQD concentration, which may be attributed to lattice structure alterations induced by the GOQD coating. These findings confirm the successful deposition of GOQDs onto the Ti6Al4V scaffold surface and validate the purity and integrity of the composite structure.

As presented in Figure 1C and D, survey spectra and high-resolution C1s spectra demonstrated clear peaks corresponding to C1s, O1s, and Ti2p. With increasing GOQD concentration, the Ti2p signal intensity gradually decreased, suggesting that the GOQDs coating partially covered the Ti6Al4V surface, thereby reducing the detectable Ti element signal. These results confirm the successful and dose-dependent loading of GOQDs on the Ti6Al4V scaffolds. Moreover, the XPS findings are consistent with previous literature reports,[42] further supporting the conclusion that GOQD coating modifies the surface elemental composition and distribution of Ti6Al4V implants.

Following the coating of Ti6Al4V scaffolds with varying concentrations of GOQDs, the FTIR spectra (Figure 1E) revealed characteristic peaks in the range of 1100–1600 cm^{-1} corresponding to C=O stretching vibrations, and a broad O–H absorption band near 3450 cm^{-1}. These findings indicate the successful incorporation of GOQDs onto the Ti6Al4V scaffold surface. Moreover, the presence of GOQDs increased the surface content of hydroxyl, carbonyl, and unsaturated double bond functional groups on the Ti6Al4V scaffolds, potentially enhancing their biocompatibility. This enhancement is likely due to chemical interactions between oxygen-containing functional groups

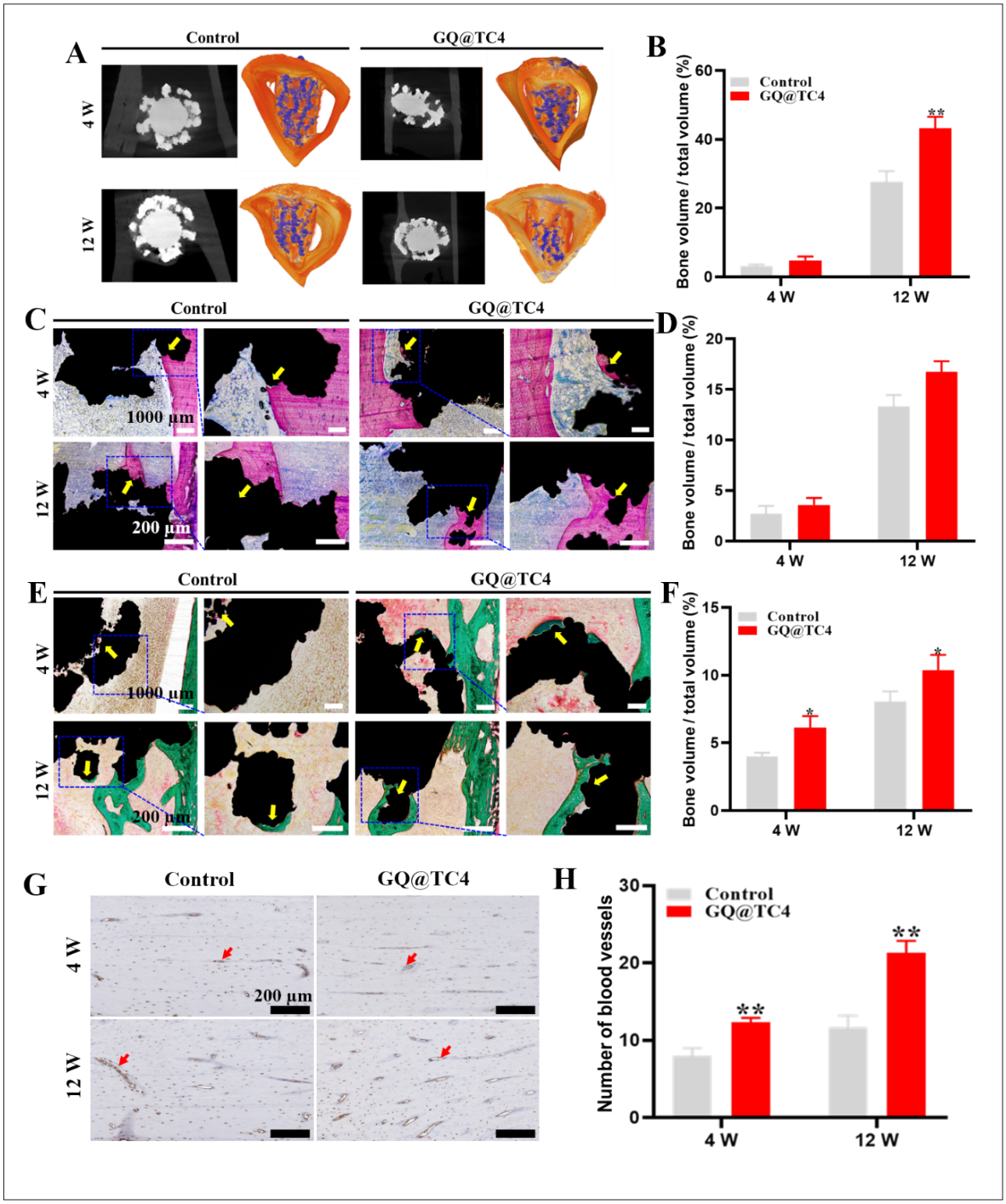

Figure 6. *In vivo* evaluation of osteogenic and angiogenic performance of the scaffolds. (A) 3D-reconstructed micro-CT images of scaffolds implanted in rabbit femurs for 4 and 12 weeks (W); the blue color indicates the Ti6Al4V scaffold, while the yellow color represents newly formed bone tissue. (B) BV/TV of different scaffolds based on micro-CT analysis. (C) H&E staining images of undecalcified sections at weeks 4 and 12 post-implantation; the red area indicates bone tissue, the black area represents the Ti6Al4V scaffold, and the yellow arrows indicate newly formed bone. (D) Quantitative analysis of BV/TV from H&E-stained sections. (E) Masson's trichrome staining images of undecalcified sections at weeks 4 and 12 post-implantation; the green area represents bone tissue, the black area represents the Ti6Al4V scaffold, and the yellow arrows indicate newly formed bone. (F) Quantitative analysis of BV/TV from Masson-stained sections. (G) Immunohistochemical images of CD31 staining at weeks 4 and 12 post-implantation, with red arrows indicating newly formed blood vessels. (H) Quantitative comparison of microvessel density among different scaffold groups. $n = 3$; $^{*}p < 0.05$ and $^{**}p < 0.01$, compared to the control. Scale bars: 1000 μm (C and E, top); 200 μm (C and E, bottom); 200 μm G. Abbreviations: BV/TV, bone volume/total volume; CT, computed tomography; H&E, hematoxylin and eosin.

on the GOQDs and the native surface functionalities of the Ti6Al4V scaffold, resulting in enriched surface chemistry.

In the context of bone repair materials, *in vitro* biological performance evaluation serves as a critical step in understanding the material–cell interactions that mimic *in vivo* bone regeneration processes. Bone scaffolds not only provide a mechanical and spatial framework for cellular adhesion, migration, proliferation, and differentiation, but also actively modulate the local microenvironment and intercellular signaling, thereby triggering a cascade of osteogenic events essential for effective bone regeneration. Thus, *in vitro* studies of biological responses are indispensable for guiding the rational design, optimization, and application of bone regenerative materials.

Upon implantation, bone repair scaffolds release bioactive components into the surrounding milieu, influencing cellular behavior through dynamic interactions with resident cells. To simulate this process, we prepared extract solutions from GOQD-functionalized porous scaffolds using complete culture medium and subsequently co-cultured these extracts with BMSCs and HUVECs.

Previous studies have demonstrated that graphene and its derivatives promote BMSC proliferation and differentiation.[31,43] Our earlier work also confirmed that GOQDs possess a strong capacity to enhance BMSC activity.[32] However, the impact of GOQD-coated titanium alloy scaffolds at different concentrations on cellular behavior remained unclear. In this study, extract solutions derived from scaffolds coated with varying concentrations of GOQDs were used to treat BMSCs, and cell proliferation was assessed using CCK-8 assays (Figure 2C). The results indicated that BMSC proliferation decreased progressively with increasing GOQD concentration. Notably, the GQ0.1@TC4 group consistently exhibited the highest proliferation rates on days 1, 3, 5, and 7 compared to the other groups. These findings indicate that while low concentrations of GOQDs can enhance BMSC proliferation, 0.1 μg/mL GOQDs (GQ0.1@TC4 group) offer the most favorable outcome, highlighting the importance of optimizing GOQD dosage for maximizing bioactivity.

The promotion of BMSC proliferation and differentiation by bone repair materials is fundamentally dependent on the initial adhesion and spreading of BMSCs on the material surface, which subsequently triggers proliferation, migration, and osteogenic differentiation. The composition and surface morphology of the substrate materials were reported to influence cellular adhesion properties.[44,45] In this study, SEM observations (Figure 5A) revealed that the number of adherent cells on scaffolds decreased as the concentration of GOQDs increased. Among all groups, the GQ0.1@TC4 scaffold displayed the highest number of adherent BMSCs. This phenomenon might have been attributed to the elevated production of reactive oxygen species (ROS) induced by higher concentrations of GOQDs, which may have damaged cell structures and impaired adhesion.[46] Previous studies have reported that excessive internalization of GOQDs can lead to elevated intracellular ROS generation, mitochondrial dysfunction, and apoptosis in stem cells and endothelial cells.[47] These ROS-mediated effects are dose-dependent and are known to compromise scaffold biocompatibility and long-term safety.

Cell adhesion on material surfaces is known to be affected by the local microenvironment. Over time, cells gradually spread and form stable attachments to the scaffold via cytoskeletal proteins. These proteins not only help maintain cellular morphology but also mediate interactions with surrounding cells and materials, thereby facilitating biological signal transmission.[48] Studies have demonstrated that the chemical composition and microtopography of biomaterials could directly affect cell spreading behavior.[49] Immunofluorescence staining further implies that within the GOQD concentration range of 0.1–10 μg/mL, an inverse relationship is observed between GOQD concentration and BMSC number. The GQ0.1@TC4 group exhibited the highest BMSC count with consistently well-organized cytoskeletal structures, whereas in the GQ10@TC4 group, fewer cells were observed with noticeably shrunken cytoskeletons. These results indicated that scaffolds coated with 0.1 μg/mL GOQD more effectively promoted BMSC adhesion. A plausible mechanism could be that low concentrations of GOQDs upregulated actin expression, which facilitated transmembrane signal transduction and enhanced cell adhesion.[42,50]

Furthermore, for RT-PCR analysis, cells were harvested directly from the scaffold to better reflect the proliferation and differentiation status of adherent cells. RT-PCR results revealed that after 7 days of co-culture, the expression levels of *Bmp2*, *Ocn*, and *Alp* genes were significantly higher in the GQ0.1@TC4 group compared to the GQ1@TC4 and GQ10@TC4 groups ($p < 0.05$), indicating enhanced osteogenic differentiation. This effect may have resulted from more effective activation of membrane receptors by low-concentration GOQDs, thereby promoting stem cell proliferation and osteogenic differentiation.[50]

To assess the effect of GOQD-functionalized scaffold extracts on HUVEC proliferation, CCK-8 assays were conducted on days 1, 3, 5, and 7 after treatment. The results indicated a dose-dependent decline in HUVEC proliferation as GOQD concentration increased. The GQ0.1@TC4 group consistently displayed significantly

greater proliferation than the other groups at all time points ($p < 0.001$).

To evaluate the pro-angiogenic effects of different GOQD concentrations, a scratch assay was performed. After 24 h, nearly complete scratch closure was observed in the GQ0.1@TC4 group, significantly faster than that of the GQ1@TC4 and GQ10@TC4 groups ($p < 0.05$). In addition, the Transwell migration assay indicated that after 24 h, the GQ0.1@TC4 group exhibited the highest number of migrated cells (635 ± 59), suggesting superior migratory capacity. Tube formation assays further demonstrated that HUVECs treated with GQ0.1@TC4 extract formed significantly longer tubular structures compared to the GQ1@TC4 and GQ10@TC4 groups ($p < 0.05$). These results were consistent with previous reports, which have reported that increasing concentrations of GO and its derivatives negatively affects the angiogenic potential of HUVECs, suppressing capillary-like structure formation in a dose-dependent manner.[51,52]

The enhanced vascularization observed with 0.1 μg/mL GOQDs might have been attributed to the moderate mechanical stress imposed on HUVECs by low concentrations of GOQDs. This stress may have induced the remodeling of actin cytoskeleton into lamellipodia and filopodia, which are involved in cell membrane protrusion, extracellular matrix adhesion, and cytoplasmic contraction—all critical processes for cell migration and angiogenesis.[53,54] HIF-1α and VEGF are two critical RNA transcripts involved in the regulation of angiogenesis. HIF-1α, a transcription factor, is known to promote angiogenesis under hypoxic conditions by enhancing the transcription of VEGF.[55] VEGF functions as a key pro-angiogenic factor and signaling RNA essential for vascular development.[56]

To investigate the *in vivo* osteogenic and early angiogenic potential of the GOQD-functionalized biomimetic scaffold, a femoral defect model was established in New Zealand white rabbits. The study aimed to evaluate the scaffold's capacity to support bone formation and early-stage vascularization *in vivo*. Micro-CT analysis revealed that 12 weeks after implantation, the GQ@TC4 scaffolds featured close integration with the adjacent cortical bone, with a substantial amount of newly formed yellow bone tissue covering the scaffold surface. The BV/TV reached 43.29 ± 3.26%, suggesting that the 0.1 μg/mL GOQDs-coated scaffold effectively promoted new bone formation. These findings indicated that low concentrations of GOQDs enhanced the osteogenic performance of titanium alloy scaffolds *in vivo*. Histological analysis using H&E staining and Masson's trichrome staining corroborated the micro-CT results. At 12 weeks post-implantation, a notable increase in newly formed bone tissue was observed surrounding the GQ@TC4 scaffolds, accompanied by a significant increase in bone volume. The ability of scaffold materials to promote new bone formation after implantation is closely associated with their capacity to stimulate neovascularization. A greater number of newly formed blood vessels typically contributes to more efficient and effective bone regeneration.[57] In this study, CD31 immunohistochemical staining further confirmed enhanced vascularization. At week 12 following implantation, the GQ@TC4 group exhibited a significantly greater number of vascular lumens with relatively larger diameters compared to the control group, and the intergroup difference was statistically significant ($p < 0.05$). These results suggested that scaffolds loaded with a specific concentration of GOQDs could promote bone tissue formation by enhancing neovascularization.

Although our study demonstrated favorable short-term biocompatibility and therapeutic efficacy of GOQD-coated scaffolds, the long-term biosafety profile of GOQDs remains insufficiently characterized. The degradation kinetics of GOQDs *in vivo* remain unclear. Unlike traditional biodegradable polymers, GOQDs may undergo incomplete enzymatic or oxidative degradation, generating intermediate species whose bioactivity or toxicity is not well-defined. Furthermore, the biodistribution and clearance mechanisms remain speculative in the absence of long-term *in vivo* tracking studies. Without such data, it is difficult to predict how GOQDs behave over extended periods or after repeated implantation. To ensure safe clinical translation, future studies should incorporate long-term *in vivo* imaging, quantitative organ-level distribution assays, and immunohistochemical analysis to determine potential inflammatory responses, nanoparticle persistence, or off-target effects. Although GOQDs are known to exhibit size-dependent quantum effects, the current coating strategy primarily utilizes their surface chemical functionality rather than their intrinsic quantum properties. Future studies should explore whether the nanoscale quantum effects of GOQDs contribute directly to the biological outcomes observed. Additionally, while standard physicochemical techniques, such as XRD, XPS, and FTIR, confirmed the successful deposition of GOQDs, comprehensive characterization of the coating properties—including structural morphology, long-term stability, and quantum dot-specific features—was not fully performed. These analyses are crucial for a deeper understanding of the coating's functionality and will be essential for future optimization and translational application.

5. Conclusion

This study systematically investigated the effects of GOQDs at varying concentrations (0, 0.1, 1, and 10 μg/mL) on the

proliferation and osteogenic differentiation of BMSCs, as well as on the proliferation and angiogenic differentiation of HUVECs. The results demonstrated that 0.1 μg/mL GOQDs most effectively promoted the proliferation and functional differentiation of both cell types. Furthermore, Ti6Al4V scaffolds coated with 0.1 μg/mL GOQDs significantly enhanced *in vivo* bone and vascular tissue formation. These findings provide a theoretical basis for the application of GOQD-functionalized biomimetic porous scaffolds in the repair of bone defects.

Acknowledgments

None.

Funding

This research was supported by the National Natural Sciences Foundation of China (No. 81974146), the Guangdong Natural Sciences Foundation (No. 2023A1515012554), the Fujian Key Laboratory of Oral Diseases, School and Hospital of Stomatology, Fujian Medical University (Grant No. 2023SZ-B01), and the International Postdoctoral Exchange Fellowship Program 2023 by the Human Resources and Social Security Department of Guangdong Province.

Conflict of interest

The authors declare that they have no known competing financial interests or personal relationships that could have appeared to influence the work reported in this article.

Author contributions

Conceptualization: Duoling Xu, Chao Wang, Dongsheng Yu, Huancai Lin, Wei Zhao
Data curation: Duoling Xu, Chao Wang, Song Yang
Formal analysis: Shujun Li, Wentao Hou, Huancai Lin, Wei Zhao
Funding acquisition: Wei Zhao, Duoling Xu, Chao Wang
Investigation: Duoling Xu, Chao Wang, Song Yang, Jie Wu, Leyi Liu
Methodology: Shujun Li, Wentao Hou
Supervision: Huancai Lin, Wei Zhao
Writing – original draft: Duoling Xu, Chao Wang, Song Yang, Jie Wu, Leyi Liu
Writing – review & editing: Dongsheng Yu, Huancai Lin, Wei Zhao

Ethics approval and consent to participate

All animal procedures strictly adhered to relevant ethical guidelines and were approved by the Institutional Animal Care and Use Committee of Sun Yat-sen University (Approval No. SYSU-IACUC-2019-000169). The study was conducted in strict adherence to the ethical principles outlined by the National Institutes of Health (NIH) regarding the care and utilization of laboratory animals.

Consent for publication

Not applicable.

Availability of data

The data that support the findings of this study are available from the corresponding authors upon reasonable request.

References

1. Ding Q, Cui J, Shen H, *et al*. Advances of nanomaterial applications in oral and maxillofacial tissue regeneration and disease treatment. *Wiley Interdiscip Rev Nanomed Nanobiotechnol*. 2020;13(2):e1669.
doi: 10.1002/wnan.1669

2. Liang Y, Li M, Yang Y, Qiao L, Xu H, Guo B. pH/glucose dual responsive metformin release hydrogel dressings with adhesion and self-healing via dual-dynamic bonding for athletic diabetic foot wound healing. *ACS Nano*. 2022;16(2):3194-3207.
doi: 10.1021/acsnano.1c11040

3. Li B, Shu R, Dai W, *et al*. Bioheterojunction-engineered polyetheretherketone implants with diabetic infectious micromilieu twin-engine powered disinfection for boosted osteogenicity. *Small*. 2022;18(45):e2203619.
doi: 10.1002/smll.202203619

4. Jang HJ, Kang MS, Jang J, *et al*. Harnessing 3D printed highly porous Ti-6Al-4V scaffolds coated with graphene oxide to promote osteogenesis. *Biomater Sci*. 2024;12(21): 5491-5503.
doi: 10.1039/d4bm00970c

5. Xiao F, Ye JH, Huang CX, *et al*. Gradient gyroid Ti6Al4V scaffolds with TiO(2) surface modification: promising approach for large bone defect repair. *Biomater Adv*. 2024;161:213899.
doi: 10.1016/j.bioadv.2024.213899

6. Zarei M, Hasanzadeh Azar M, Sayedain SS, *et al*. Material extrusion additive manufacturing of poly(lactic acid)/ Ti6Al4V@calcium phosphate core-shell nanocomposite scaffolds for bone tissue applications. *Int J Biol Macromol*. 024;255:128040.
doi: 10.1016/j.ijbiomac.2023.128040

7. Zhang X, Guan S, Qiu J, *et al*. Atomic layer deposition of tantalum oxide films on 3D-printed Ti6al4v scaffolds with enhanced osteogenic property for orthopedic implants. *ACS Biomater Sci Eng*. 2023;9(7):4197-4207.
doi: 10.1021/acsbiomaterials.3c00217

8. Shah NJ, Hyder MN, Moskowitz JS, *et al*. Surface-mediated bone tissue morphogenesis from tunable nanolayered implant coatings. *Sci Transl Med*. 2013;5(191):191ra83. doi: 10.1126/scitranslmed.3005576

9. Shum JM, Gadomski BC, Tredinnick SJ, *et al*. Enhanced bone formation in locally-optimised, low-stiffness additive manufactured titanium implants: an in silico and in vivo tibial advancement study. *Acta Biomater*. 2023;156:202-213. doi: 10.1016/j.actbio.2022.04.006

10. Abaricia JO, Farzad N, Heath TJ, Simmons J, Morandini L, Olivares-Navarrete R. Control of innate immune response by biomaterial surface topography, energy, and stiffness. *Acta Biomater*. 2021;133:58-73. doi: 10.1016/j.actbio.2021.04.021

11. Ching HA, Choudhury D, Nine MJ, Abu Osman NA. Effects of surface coating on reducing friction and wear of orthopaedic implants. *Sci Technol Adv Mater*. 2014;15(1):014402. doi: 10.1088/1468-6996/15/1/014402

12. Mediero A, Frenkel SR, Wilder T, He W, Mazumder A, Cronstein BN. Adenosine A2A receptor activation prevents wear particle-induced osteolysis. *Sci Transl Med*. 2012;4(135):135ra65. doi: 10.1126/scitranslmed.3003393

13. Dinoro J, Maher M, Talebian S, *et al*. Sulfated polysaccharide-based scaffolds for orthopaedic tissue engineering. *Biomaterials*. 2019;214:119214. doi: 10.1016/j.biomaterials.2019.05.025

14. Kapat K, Srivas PK, Rameshbabu AP, *et al*. Influence of porosity and pore-size distribution in Ti(6)Al(4) V foam on physicomechanical properties, osteogenesis, and quantitative validation of bone ingrowth by micro-computed tomography. *ACS Appl Mater Interfaces*. 2017;9(45):39235-39248. doi: 10.1021/acsami.7b13960

15. Wang C, Xu D, Li S, *et al*. Effect of pore size on the physicochemical properties and osteogenesis of ti6al4v porous scaffolds with bionic structure. *ACS Omega*. 2020;5(44):28684-28692. doi: 10.1021/acsomega.0c03824

16. Wang C, Xu D, Lin L, *et al*. Large-pore-size Ti6Al4V scaffolds with different pore structures for vascularized bone regeneration. *Mater Sci Eng C Mater Biol Appl*. 1;131:112499. doi: 10.1016/j.msec.2021.112499

17. Wang C, Wu J, Liu L, *et al*. Improving osteoinduction and osteogenesis of ti6al4v alloy porous scaffold by regulating the pore structure. *Front Chem*. 2023;11:1190630. doi: 10.3389/fchem.2023.1190630

18. Lee H, Lee MK, Han G, *et al*. Customizable design of multiple-biomolecule delivery platform for enhanced osteogenic responses via 'tailored assembly system'. *Bio Des Manuf*. 2022;5(3):451-464. doi: 10.1007/s42242-022-00190-7

19. Lee MK, Lee H, Park C, *et al*. Accelerated biodegradation of iron-based implants via tantalum-implanted surface nanostructures. *Bioact Mater*. 2022;9:239-250. doi: 10.1016/j.bioactmat.2021.07.003

20. Deshmukh S, Chand A, Ghorpade R. Bio-mechanical analysis of porous Ti-6Al-4V scaffold: a comprehensive review on unit cell structures in orthopaedic application. *Biomed Phys Eng Express*. 2024;10(6):062003. doi: 10.1088/2057-1976/ad8202

21. Unsworth T. Proceedings of the Institution of Mechanical Engineers Part H. *Proc Inst Mech Eng H*. 2008;222(7):i. doi: 10.1177/095441190822200701

22. Awonusi BO, Li H, Yin Z, Zhao J, Yang K, Li J. Surface modification of Zn-Cu Alloy with heparin nanoparticles for urinary implant applications. *ACS Appl Bio Mater*. 2024;7(3):1748-1762. doi: 10.1021/acsabm.3c01177

23. Ehlert M, Radtke A, Bartmanski M, Piszczek P. Evaluation of the cathodic electrodeposition effectiveness of the hydroxyapatite layer used in surface modification of Ti6Al4V-based biomaterials. *Materials (Basel)*. 2022;15(19):6925. doi: 10.3390/ma15196925

24. Teixeira-Santos R, Belo S, Vieira R, Mergulhao FJM, Gomes LC. Graphene-based composites for biomedical applications: surface modification for enhanced antimicrobial activity and biocompatibility. *Biomolecules*. 2023;13(11):1571. doi: 10.3390/biom13111571

25. Kang MS, Jeong SJ, Lee SH, *et al*. Reduced graphene oxide coating enhances osteogenic differentiation of human mesenchymal stem cells on Ti surfaces. *Biomater Res*. 2021;25(1):4. doi: 10.1186/s40824-021-00205-x

26. Li P, Di Stasio F, Eda G, *et al*. Luminescent properties of a water-soluble conjugated polymer incorporating graphene-oxide quantum dots. *Chemphyschem*. 2015;16(6):1258-1262. doi: 10.1002/cphc.201402744

27. Liu G, Zhang K, Ma K, Care A, Hutchinson MR, Goldys EM. Graphene quantum dot-based "switch-on" nanosensors for intracellular cytokine monitoring. *Nanoscale*. 2017;9(15):4934-4943. doi: 10.1039/c6nr09381g

28. Yang X, Zhao Q, Chen Y, *et al*. Effects of graphene oxide and graphene oxide quantum dots on the osteogenic differentiation of stem cells from human exfoliated deciduous teeth. *Artif Cells Nanomed Biotechnol*. 2019;47(1):822-832. doi: 10.1080/21691401.2019.1576706

29. Lin L, Zheng Y, Wang C, Li P, Xu D, Zhao W. Concentration-dependent cellular uptake of graphene oxide quantum dots promotes the odontoblastic differentiation of dental pulp cells via the AMPK/mTOR pathway. *ACS Omega*. 2023;8(6):5393-5405. doi: 10.1021/acsomega.2c06508

30. Liao TT, Deng QY, Wu BJ, *et al*. Dose-dependent cytotoxicity evaluation of graphite nanoparticles for diamond-like carbon film application on artificial joints. *Biomed Mater*. 2017;12(1):015018.
doi: 10.1088/1748-605X/aa52ca

31. Qiu J, Li D, Mou X, *et al*. Effects of graphene quantum dots on the self-renewal and differentiation of mesenchymal stem cells. *Adv Healthc Mater*. 2016;5(6):702-710.
doi: 10.1002/adhm.201500770

32. Xu D, Wang C, Wu J, *et al*. Effects of low-concentration graphene oxide quantum dots on improving the proliferation and differentiation ability of bone marrow mesenchymal stem cells through the Wnt/beta-catenin signaling pathway. *ACS Omega*. 2022;7(16):13546-13556.
doi: 10.1021/acsomega.1c06892

33. Xie H, Cao T, Rodriguez-Lozano FJ, Luong-Van EK, Rosa V. Graphene for the development of the next-generation of biocomposites for dental and medical applications. *Dental Mater*. 2017;33(7):765-774.
doi: 10.1016/j.dental.2017.04.008

34. Pruna A, Cembrero J, Pullini D, Mocioiu AM, Busquets-Mataix D. Effect of reduced graphene oxide on photocatalytic properties of electrodeposited ZnO. *Appl Phys A Mater*. 2017;123(12):792.
doi: 10.1007/s00339-017-1424-1

35. Yan X, An N, Zhang Z, *et al*. Graphene oxide quantum dots-preactivated dental pulp stem cells/GelMA facilitates mitophagy-regulated bone regeneration. *Int J Nanomed*. 2024;19:10107-10128.
doi: 10.2147/IJN.S480979

36. An N, Yan X, Qiu Q, *et al*. Human periodontal ligament stem cell sheets activated by graphene oxide quantum dots repair periodontal bone defects by promoting mitochondrial dynamics dependent osteogenic differentiation. *J Nanobiotechnol*. 2024;22(1):133.
doi: 10.1186/s12951-024-02422-7

37. Jia ZJ, Shi YY, Xiong P, *et al*. From solution to biointerface: graphene self-assemblies of varying lateral sizes and surface properties for biofilm control and osteodifferentiation. *ACS Appl Mater Inter*. 2016;8(27):17151-17165.
doi: 10.1021/acsami.6b05198

38. Kang ES, Song I, Kim DS, *et al*. Size-dependent effects of graphene oxide on the osteogenesis of human adipose-derived mesenchymal stem cells. *Colloid Surface B*. 2018;169:20-29.
doi: 10.1016/j.colsurfb.2018.04.053

39. Li XJ, Lin KL, Wang ZL. Enhanced growth and osteogenic differentiation of MC3T3-E1 cells on Ti6Al4V alloys modified with reduced graphene oxide. *Rsc Adv*. 2017;7(24):14430-14437.
doi: 10.1039/c6ra25832h

40. Li D, Dai D, Wang J, Zhang C. Honeycomb bionic graphene oxide quantum dot/layered double hydroxide composite nanocoating promotes osteoporotic bone regeneration via activating mitophagy. *Small*. 2024;20(50):e2403907.
doi: 10.1002/smll.202403907

41. Ha HD, Jang MH, Liu F, Cho YH, Seo TS. Upconversion photoluminescent metal ion sensors via two photon absorption in graphene oxide quantum dots. *Carbon*. 2015;81:367-375.
doi: 10.1016/j.carbon.2014.09.069

42. Qiu JJ, Geng H, Wang DH, *et al*. Layer-number dependent antibacterial and osteogenic behaviors of graphene oxide electrophoretic deposited on titanium. *ACS Appl Mater Inter*. 2017;9(14):12253-12263.
doi: 10.1021/acsami.7b00314

43. Chen X, Sun Z, Peng X, *et al*. Graphene oxide/black phosphorus functionalized collagen scaffolds with enhanced near-infrared controlled in situ biomineralization for promoting infectious bone defect repair through PI3K/Akt pathway. *ACS Appl Mater Interfaces*. 2024;16(38):50369-50388.
doi: 10.1021/acsami.4c10284

44. Kiroshka VV, Petrova VA, Chernyakov DD, *et al*. Influence of chitosan-chitin nanofiber composites on cytoskeleton structure and the proliferation of rat bone marrow stromal cells. *J Mater Sci Mater M*. 2017;28(1):21.
doi: 10.1007/s10856-016-5822-2

45. Xue DT, Chen EM, Zhong HM, *et al*. Immunomodulatory properties of graphene oxide for osteogenesis and angiogenesis. *Int J Nanomed*. 2018;13:5799-5810.
doi: 10.2147/Ijn.S170305

46. Zhou J, Zhao L. Multifunction Sr, Co and F co-doped microporous coating on titanium of antibacterial, angiogenic and osteogenic activities. *Sci Rep*. 2016;6:29069.
doi: 10.1038/srep29069

47. Jiang X, Chen X, Li Q, *et al*. Synergistic effects of polydopamine-coated reduced graphene oxide on osteogenesis and anti-inflammation in periodontitis. *J Mater Sci Mater Med*. 2025;36(1):51.
doi: 10.1007/s10856-025-06905-3

48. Ma R, Tang SC, Tan HL, *et al*. Preparation, characterization, and in vitro osteoblast functions of a nano-hydroxyapatite/polyetheretherketone biocomposite as orthopedic implant material. *Int J Nanomed*. 2014;9:3949-3961.
doi: 10.2147/Ijn.S67358

49. Sankar D, Shalumon KT, Chennazhi KP, Menon D, Jayakumar R. Surface plasma treatment of poly(caprolactone) micro, nano, and multiscale fibrous scaffolds for enhanced osteoconductivity. *Tissue Eng Pt A*. 2014;20(11-12):1689-1702.
doi: 10.1089/ten.tea.2013.0569

50. Park JB, Ahn JY, Yang WS, *et al*. Stacked graphene with nanoscale wrinkles supports osteogenic differentiation of human adipose-derived stromal cells. *2D Mater*. 2021;8(2):025034.
doi: 10.1088/2053-1583/abe105

51. Lamalice L, Le Boeuf F, Huot J. Endothelial cell migration during angiogenesis. *Circ Res*. 2007;100(6):782-794. doi: 10.1161/01.RES.0000259593.07661.1e

52. Wang Q, Chen MC, Schafer NP, *et al*. Assemblies of calcium/calmodulin-dependent kinase II with actin and their dynamic regulation by calmodulin in dendritic spines. *Proc Natl Acad Sci U S A*. 2019;116(38): 18937-18942. doi: 10.1073/pnas.1911452116

53. Cota Teixeira S, Silva Lopes D, Santos da Silva M, *et al*. Pentachloropseudilin impairs angiogenesis by disrupting the actin cytoskeleton, integrin trafficking and the cell cycle. *Chembiochem*. 2019;20(18):2390-2401. doi: 10.1002/cbic.201900203

54. Yadunandanan Nair N, Samuel V, Ramesh L, Marib A, David DT, Sundararaman A. Actin cytoskeleton in angiogenesis. *Biol Open*. 2022;11(12):bio058899. doi: 10.1242/bio.058899

55. Nakayama M, Nakayama A, van Lessen M, *et al*. Spatial regulation of VEGF receptor endocytosis in angiogenesis. *Nat Cell Biol*. 2013;15(3):249-260. doi: 10.1038/ncb2679

56. Soker S, Machado M, Atala A. Systems for therapeutic angiogenesis in tissue engineering. *World J Urol*. 2000;18(1):10-18. doi: 10.1007/Pl00007070

57. Liu WC, Chen SH, Zheng LZ, Qin L. Angiogenesis assays for the evaluation of angiogenic properties of orthopaedic biomaterials-a general review. *Adv Healthc Mater*. 2017;6(5):1600434. doi: 10.1002/adhm.201600434